Turkish Journal of Electrical Engineering & Computer Sciences

http://journals.tubitak.gov.tr/elektrik/

Research Article

Turk J Elec Eng & Comp Sci
(2014) 22: 546 – 561

doi:10.3906/elk-1208-51

An efficient approach to the local optimization of finite electromagnetic band-gap structures

David DUQUE*, Vito LANCELLOTTI, Bastiaan Pieter DE HON, Antonius TIJHUIS
Faculty of Electrical Engineering, Technical University of Eindhoven, Eindhoven, the Netherlands

Received: 14.08.2012 • **Accepted:** 21.11.2012 • **Published Online:** 21.03.2014 • **Printed:** 18.04.2014

Abstract: We propose a methodology based on linear embedding via Green's operators (LEGO) and the eigencurrent expansion method (EEM) to efficiently deal with and locally optimize 2-D electrically large electromagnetic band-gap (EBG) structures. In LEGO terminology, the composite EBG structure is broken up (diakopted) into constitutive elements called "bricks" that we characterize through scattering operators by invoking Love's equivalence principle, while, at the same time, the electromagnetic interaction among the bricks is captured by transfer operators. The resulting electromagnetic problem is then succinctly formulated through an integral equation involving the total inverse scattering operator $\mathcal{S}^{-1}$ of the structure. To perform local optimization, the formulation of the problem allows for variations of the electromagnetic properties and the shape of a set of objects in the EBG structure with respect to those of the others, thereby allowing us to tune a compact designated domain within a large one. Finally, the method of moments and the EEM are applied to achieve a considerable reduction in memory use for the overall problem.

Key words: Computational electromagnetics, method of moments, linear embedding via Green's operators, eigencurrent expansion method, integral equations

1. Introduction

Let us consider a periodic array of objects with electromagnetic contrast; if the spatial period over which this contrast varies is comparable with the wavelength of the incident electromagnetic field, then intricate scattered fields and electromagnetic band-gaps (i.e. forbidden frequency bands where no electromagnetic wave can propagate within the structure) may occur. Such arrays of objects in 2-D and 3-D are called electromagnetic band-gap (EBG) structures.

EBG structures have over the past decades gained considerable attention in the physics and engineering communities because of their potential to control the propagation of electromagnetic waves by exciting localized electromagnetic (EM) modes within a band-gap upon introducing "defects" in the EBG structure. This property is exploited now in many applications such as antenna structures, waveguides, filters, planar reflectors, infrared wavelengths, integrated circuits, and high- and low-Q resonators [1]. Numerous approaches have been used recurrently to analyze EBG structures. For the sake of brevity, we briefly describe them while referring the reader to the corresponding literature. The plane-wave expansion method [2] has been used extensively for the analysis of fully periodic EBG structures. Several transfer-matrix methods have also been developed [3] [4]. These methods are more flexible than the plane-wave method, in that periodicity is no longer required in one direction. Nevertheless, transfer-matrix methods are not inherently stable [5]. The finite difference time domain

*Correspondence: d.j.duque@tue.nl

(FDTD) method [6] is commonly used to simulate and to compute band-gap diagrams for photonic crystal (PhC) and 2-D metal photonic band-gap cavities [7]. The inherent problem is that for a sufficiently fine grid, the FDTD may become computationally demanding when the electric size of the problem increases. More recently, the transmission line method (TLM) has been used to compute far-field radiation of antennas embedded in 1-D EBG of multilayer slabs [8]. Using the reciprocity theorem [9], the TLM transforms the far-field problem into the evaluation of the field in the 1-D EBG structure due to an incident plane wave and solves it using a cascaded transmission line circuit derived from the multilayer structure. The scattering matrix method (originated from that of cascading networks in circuit theory) has been used to analyze periodic structures composed of multiple layers of frequency-selective surfaces [10]. The method considerably reduces the computing time as compared to conventional methods, which calculate the overall scattering from the structure. This cascading approach is well suited for design optimization, because it is possible to evaluate the effect of any change in one layer without repeating the whole computing process. The diffraction grating method, for example, has been used to design and characterize 2-D EBG structures [1]. In this method one considers the 2-D EBG material as a stack of periodic grids of rods (i.e. as a stack of 1-D diffraction gratings) and then a rigorous full-wave diffraction theory is used to solve the problem. What is more, to alleviate the need for 3-D calculations in the analysis of slab-based 2-D EBG structures, several 2-D modeling approaches have also been developed and proposed [11] [12] [13]. In these methods, a dimensionality reduction (from 3-D to 2-D) of the problem is often performed. Thus, the location of band gaps and other spectral features are well predicted. There are several other methods to analyze, characterize, and optimize 2-D EBG structures, which we mention for the sake of brevity. Among them we have the effective medium theory [14], the eigenvector expansion method [15], the finite element method (FEM) [16], and the array scanning method [17].

We can note that in most of the methods mentioned above, the field calculation is performed either directly for the entire structure or for well-defined parts of the EBG (i.e. an EBG layer, an EBG implant) that are subsequently combined. For structures with a predominantly periodic conformation, the latter approach has 2 obvious advantages: the intermediate problems are computationally much smaller than the complete problem, and the intermediate results can be reused as building blocks for a variety of composite structures. The method that we will propose below is akin to the ideas briefly outlined above, in the sense that our method is a multiple-step method based on a scattering formalism, whose purpose is to reinforce and expand the available list of numerical tools for analyzing large 2-D EBG structures.

In contrast to the methods discussed above, we propose linear embedding via Green's operators (LEGO) combined with the eigencurrent expansion method (EEM). The LEGO approach is a domain decomposition method that uses field diakoptics [18] by invoking either Love's equivalence principle [9] [19] or Schelkunoff's equivalence principle [20] to tackle an electromagnetic problem. As a matter of fact, in LEGO a composite structure is broken up (diakopted) into individual bricks, each containing an object or set of objects forming the EBG structure. Each brick is then characterized by its scattering operator and the electromagnetic interaction among the bricks is captured by transfer operators. Hence, LEGO shares the very same idea of first solving a small problem before a larger one by tearing apart the structure into pieces with methods such as the nested equivalence principle algorithm [21] and the equivalence principle algorithm [22]. The idea of isolating a body with different electromagnetic properties from the surroundings within a designated domain as a "target" for optimization was already applied in [5] in a former 2-D implementation of LEGO. Nevertheless, in [5], the contribution of the large fixed part of the 2-D EBG structure was obtained by computing its total scattering operator through a cascade of successive embedding steps where 2 elemental scattering operators are combined

to form a new scattering operator commonly twice as big; moreover, the variable under optimization is tuned through a sweep, rather than defining a formal cost function. This approach clearly has 2 disadvantages. First, the size of the elemental scattering operators doubles at each iteration step, and hence an application of the embedding procedure to a large problem would soon cause a rapid drain of the memory resources of most computers, consequently limiting the electric size of the structure that can be modeled. Second, no guarantee of finding the optimal point for the variable under optimization can be given when using a sweep.

To get around these hurdles, we combine the EEM with LEGO. Briefly speaking, the idea behind the EEM is to use a set of basis functions that allows for an efficient representation of the pertinent operator eigenfunctions. These ad hoc functions, as we will show, are locally entire domain functions that effectively allow us to compress the original problem, thus enabling us to handle relatively large structures. Certainly, a 2-D implementation of the LEGO-EEM approach constitutes not only a substantial improvement over [5] but also finds its value in a wide range of practical applications. For example, most of the electromagnetic problems derived from 2-D EBG structures are essentially 2-D in nature; thereby, such implementation inherently brings several advantages. Among them, we can mention the possibility of analyzing structures bigger than what can be dealt with in a 3-D implementation. We do need fewer unknowns per brick, and thereby saving of computer memory and faster characterization of 2-D EBG structures can be achieved. Integral operators are less complicated in a 2-D than in a 3-D case. Finally, many structures, such as those encountered in optics, often allow for a hybrid 2-D/3-D analysis, which is the natural extension of the 2-D case [23].

We have presented the early implications of our computational scheme at conferences. In particular, in [24] we built upon the efficient and robust strategy presented in the current manuscript for optimizing electromagnetic band-gap applications by considering a PhC-based drop filter. In [23] we explored the possibility of extending the method into a mixed 2-D/3-D modeling scheme. We have reserved this manuscript for providing the solid foundation and systematic mathematical underpinning and the level of details required to support and reproduce the results laid out in these conference contributions and for future work. In this paper, we extend the total inverse scattering operator introduced in [25] for the worthy instance of 2 general interacting structures, one of them having varying parameters that we identify as the target to be optimized. Based on this extended scattering operator, we develop an efficient strategy for the local optimization of 2-D EBG structures.

The paper is organized as follows. In Section 2, we briefly introduce the LEGO approach and we formulate the optimization problem of a 2-D EBG structure using LEGO. In Section 3, we present the EEM and we combine it with LEGO in order for it to be used for design optimization, which is the distinctive idea of this work. In Section 4, we present a numerical example to show how to effectively optimize a 2-D EBG polarization splitter using LEGO-EEM. In Section 5, conclusions are given.

2. The formulation

We consider a 2-D EBG structure comprising $N_{\mathrm{B}} + N_{\mathrm{T}}$ elements, which are immersed in a homogeneous background medium as shown in Figure 1. Here, N_{B} is the number of elements whose shape and properties are supposed not to change. We call these elements as a whole the "fixed" part of the structure. N_{T} is the number of elements whose composition and shape has to be optimized, and we refer to them as the "target". A time-harmonic dependence ($\exp(\mathrm{j}\omega t)$) is assumed throughout and suppressed. In LEGO, we start solving the problem by "tearing apart" the structure into constituent elements, as also done in [26] and [27] for antenna problems. We then embed each element in a bounded domain $\mathcal{D}_k,\ k = 1, \cdots, N_{\mathrm{B}} + N_{\mathrm{T}}$, as also shown in Figure 1, and we refer to $\mathcal{D}_k$ as LEGO bricks. We characterize electromagnetically each brick $\mathcal{D}_k$ independently of one

another and of the external sources by means of scattering operators $\mathcal{S}_{kk}$ [5] [25] [28], which in the formalism of Love's equivalence principle [19] [9] maps equivalent incident currents $q_k^{\mathrm{i}} = \left[\boldsymbol{J}_k^{\mathrm{i}}, \boldsymbol{M}_k^{\mathrm{i}}\right]^{\mathrm{T}}$ on $\partial\mathcal{D}_k^-$ into equivalent scattered currents $q_k^{\mathrm{s}} = [\boldsymbol{J}_k^{\mathrm{s}}, \boldsymbol{M}_k^{\mathrm{s}}]^{\mathrm{T}}$ on $\partial\mathcal{D}_k^+$, and to capture the multiple scattering taking place in the structure, we use the dimensionless transfer operator $\mathcal{T}_{kn}$ between any 2 bricks $\mathcal{D}_k$ and $\mathcal{D}_n$ [5], [25], [28], as depicted in Figure 1.

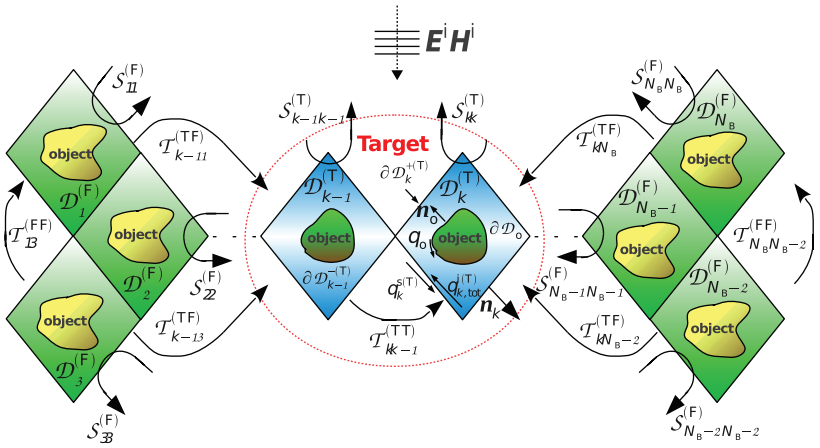

Figure 1. Optimization with LEGO: A large 2-D EBG structure is divided into small subdomains that are characterized by the scattering operator $\mathcal{S}_{kk}$. The multiple scattering taking place in the structure is captured by transfer operators $\mathcal{T}_{kn}$. A part of the structure with possible varying parameters is identified as the target in the optimization.

2.1. An integral equation for optimization

We formulate the problem in terms of an equation to be solved for q_k^{s} rather than build numerically the total scattering operator of the structure through a cascade of subsequent embedding steps, as was done in [5]. To this end, we may relate q_k^{s} with the total incident equivalent current $q_{k,\mathrm{tot}}^{\mathrm{i}}$ as follows:

$$\begin{aligned} q_k^{\mathrm{s(F)}} &= \mathcal{S}_{kk}^{(\mathrm{F})} q_{k,\mathrm{tot}}^{\mathrm{i(F)}}, \quad k = 1, \ldots, N_{\mathrm{B}}, \\ &= \mathcal{S}_{kk}^{(\mathrm{F})} \left(q_k^{\mathrm{i(F)}} + \sum_{\substack{n=1 \\ n \neq k}}^{N_{\mathrm{B}}} q_{k(n)}^{\mathrm{i(F)}} + \sum_{m=1}^{N_{\mathrm{T}}} q_{k(m)}^{\mathrm{i(F)}} \right), \end{aligned} \tag{1}$$

$$\begin{aligned} q_l^{\mathrm{s(T)}} &= \mathcal{S}_{ll}^{(\mathrm{T})} q_{l,\mathrm{tot}}^{\mathrm{i(T)}}, \quad l = 1, \ldots, N_{\mathrm{T}}, \\ &= \mathcal{S}_{ll}^{(\mathrm{T})} \left(q_l^{\mathrm{i(T)}} + \sum_{n=1}^{N_{\mathrm{B}}} q_{l(n)}^{\mathrm{i(T)}} + \sum_{\substack{m=1 \\ m \neq l}}^{N_{\mathrm{T}}} q_{l(m)}^{\mathrm{i(T)}} \right), \end{aligned} \tag{2}$$

where the superscript $^{\mathrm{F(T)}}$ denotes whether the brick k (l) is in the fixed (target) part of the 2-D EBG. We see in Eqs. (1) and (2) that $q_{k,\mathrm{tot}}^{\mathrm{i(F)}}$ ($q_{l,\mathrm{tot}}^{\mathrm{i(T)}}$) is the sum of 3 contributions.

1. $q_k^{\mathrm{i(F)}}$ and $q_l^{\mathrm{i(T)}}$ are the equivalent currents on $\partial\mathcal{D}_k^{-(\mathrm{F})}$ and $\partial\mathcal{D}_l^{-(\mathrm{T})}$ radiating the impressed incident field inside $\mathcal{D}_k^{(\mathrm{F})}$ and $\mathcal{D}_l^{(\mathrm{T})}$.

2. $\sum_{\substack{n=1\\n\neq k}}^{N_\mathrm{B}} q_{k(n)}^{\mathrm{i(F)}}$ and $\sum_{\substack{m=1\\m\neq l}}^{N_\mathrm{T}} q_{l(m)}^{\mathrm{i(T)}}$ are the additional equivalent incident currents on $\partial\mathcal{D}_k^{-(\mathrm{F})}$ and $\partial\mathcal{D}_l^{-(\mathrm{T})}$ due to the multiple scattering that takes place in the fixed structure and the target.

3. $\sum_{m=1}^{N_\mathrm{T}} q_{k(m)}^{\mathrm{i(F)}}$ and $\sum_{n=1}^{N_\mathrm{B}} q_{l(n)}^{\mathrm{i(T)}}$ are additional equivalent incident currents on $\partial\mathcal{D}_k^{-(\mathrm{F})}$ and $\partial\mathcal{D}_l^{-(\mathrm{T})}$ due to the interaction between the fixed structure and the target.

The additional equivalent incident currents $q_{k(n)}^{\mathrm{i(F)}}$, $q_{l(n)}^{\mathrm{i(T)}}$, $q_{k(m)}^{\mathrm{i(F)}}$, and $q_{l(m)}^{\mathrm{i(T)}}$ in Eqs. (1) and (2) may be expressed in terms of the equivalent scattered currents $q_n^{\mathrm{s(F)}}$ and $q_m^{\mathrm{s(T)}}$ by means of the pertinent set of transfer operators $\mathcal{T}_{kn}^{(\mathrm{FF})}$, $\mathcal{T}_{ln}^{(\mathrm{TF})}$, $\mathcal{T}_{km}^{(\mathrm{FT})}$, and $\mathcal{T}_{lm}^{(\mathrm{TT})}$. Thus, we may write Eqs. (1) and (2) as:

$$\mathcal{S}_{kk}^{-1(\mathrm{F})} q_k^{\mathrm{s(F)}} = q_k^{\mathrm{i(F)}} + \sum_{\substack{n=1\\n\neq k}}^{N_\mathrm{B}} \mathcal{T}_{kn}^{(\mathrm{FF})} q_n^{\mathrm{s(F)}} + \sum_{m=1}^{N_\mathrm{T}} \mathcal{T}_{km}^{(\mathrm{FT})} q_m^{\mathrm{s(T)}}, \tag{3}$$

$$\mathcal{S}_{ll}^{-1(\mathrm{T})} q_l^{\mathrm{s(T)}} = q_l^{\mathrm{i(T)}} + \sum_{n=1}^{N_\mathrm{B}} \mathcal{T}_{ln}^{(\mathrm{TF})} q_n^{\mathrm{s(F)}} + \sum_{\substack{m=1\\m\neq l}}^{N_\mathrm{T}} \mathcal{T}_{lm}^{(\mathrm{TT})} q_m^{\mathrm{s(T)}}. \tag{4}$$

We complete the formulation by solving the $N_\mathrm{B} + N_\mathrm{T}$ BIEs stated in Eqs. (3) and (4). To do so, we define the global transfer operators $\boldsymbol{\mathcal{T}}^{(\mathrm{FT})}$ and $\boldsymbol{\mathcal{T}}^{(\mathrm{TF})}$ between the fixed structure and the target such that $\left(\boldsymbol{\mathcal{T}}^{(\mathrm{FT})}\right)_{km} = \mathcal{T}_{km}^{(\mathrm{FT})}$ and $\left(\boldsymbol{\mathcal{T}}^{(\mathrm{TF})}\right)_{ln} = \mathcal{T}_{ln}^{(\mathrm{TF})}$, and we use the definition of the inverse scattering operator for a single structure [25]. With these definitions, Eqs. (3) and (4) can be written succinctly as:

$$\begin{aligned} \boldsymbol{\mathcal{S}}^{-1(\mathrm{F})} \boldsymbol{q}^{\mathrm{s(F)}} - \boldsymbol{\mathcal{T}}^{(\mathrm{FT})} \boldsymbol{q}^{\mathrm{s(T)}} &= \boldsymbol{q}^{\mathrm{i(F)}}, \\ \boldsymbol{\mathcal{S}}^{-1(\mathrm{T})} \boldsymbol{q}^{\mathrm{s(T)}} - \boldsymbol{\mathcal{T}}^{(\mathrm{TF})} \boldsymbol{q}^{\mathrm{s(F)}} &= \boldsymbol{q}^{\mathrm{i(T)}}, \end{aligned} \tag{5}$$

with

$$\left(\boldsymbol{\mathcal{S}}^{-1(\mathrm{F,T})}\right)_{kp} = \begin{cases} \mathcal{S}_{kk}^{-1(\mathrm{F,T})} & k = p, \\ -\mathcal{T}_{kp}^{(\mathrm{FF,TT})} & k \neq p, \end{cases} \tag{6}$$

$$\boldsymbol{q}^{\mathrm{s,i(F)}} = \begin{bmatrix} q_1^{\mathrm{s,i(F)}} \\ \vdots \\ q_{N_\mathrm{B}}^{\mathrm{s,i(F)}} \end{bmatrix}, \qquad \boldsymbol{q}^{\mathrm{s,i(T)}} = \begin{bmatrix} q_1^{\mathrm{s,i(T)}} \\ \vdots \\ q_{N_\mathrm{T}}^{\mathrm{s,i(T)}} \end{bmatrix}. \tag{7}$$

The system in Eq. (5), together with the definitions in Eqs. (6) and (7), constitute the EM formulation of the problem depicted in Figure 1. Moreover, the system matrix may be interpreted as an extension of the inverse scattering operator introduced in [25] for the notable instance when 2 generic structures interact, and it can be easily generalized for an arbitrary number of structures. Note that in the case of an optimization, the corresponding terms associated to the target are the only ones to be recomputed.

3. The eigencurrent expansion method

The system in Eq. (5) is a closed-form expression that fully describes the electromagnetic interaction between 2 arbitrary structures. Nonetheless, we observe that if we were to try to solve Eq. (5) directly using the standard MoM, in general we would fail unless we were dealing with a moderate-size electromagnetic problem. This is because the resulting system matrix may soon become too large to be stored and solved. Hence, in order to solve Eq. (5) efficiently we apply the EEM as described in [25]. Nevertheless, since we still have to fit the EEM to the system in Eq. (5), we provide a short overview of it.

3.1. Overview

The idea behind the EEM is to expand $\boldsymbol{q}^{\mathrm{s(F,T)}}$ and $\boldsymbol{q}^{\mathrm{i(F,T)}}$ in Eq. (7) using a set $\mathbb{E}$ of functions that allows for an efficient representation of the true eigenfunctions, say $\{\boldsymbol{s}_m^{(k)}\}$, $m \in \mathbb{N}$, of the system operator in Eq. (5). We dub these functions eigencurrents because, in light of Eq. (5), there is a mapping from currents to currents. To figure out what the set $\mathbb{E}$ should be, we neglect for the moment the multiple scattering taking place in the structure of Figure 1. This implies 2 things: 1) the transfer operators in Eq. (6) vanish, and 2) the global transfer operators in Eq. (5) also vanish. In this ideal case, the eigencurrents $\{\boldsymbol{e}_m^{(k)}\}$ of $\mathrm{diag}\left\{\boldsymbol{\mathcal{S}}^{-1(\mathrm{F})}, \boldsymbol{\mathcal{S}}^{-1(\mathrm{T})}\right\}$ in Eq. (5) are formed by a mere juxtaposition of the eigencurrents $\{\boldsymbol{u}_m^{(k)}\}$ of $\mathcal{S}_{kk}^{-1}$, $\forall k = 1, \ldots, N_{\mathrm{B}} + N_{\mathrm{T}}$. Symbolically, this reads as

$$\boldsymbol{e}_m^{(k)} = \left[\boldsymbol{0}, \cdots, \boldsymbol{u}_m^{(k)}, \cdots, \boldsymbol{0}\right]^T, \; m \in \mathbb{N}, \tag{8}$$

where $\boldsymbol{u}_m^{(k)}$ is the mth eigenfunction of $\mathcal{S}_{kk}$. In addition, we observe that $\boldsymbol{e}_m^{(k)}$ is zero over all $\partial\mathcal{D}_n$, $n \neq k$, except on $\partial\mathcal{D}_k$ where it coincides with $\boldsymbol{u}_m^{(k)}$. Thereby, $\boldsymbol{e}_m^{(k)}$ will approximate a true eigenfunction $\boldsymbol{s}_m^{(k)}$ insofar as the mutual coupling between any 2 bricks can be neglected. Following this idea, we may then expect the higher order eigenfunctions $\boldsymbol{e}_m^{(k)}$ –those with the smaller eigenvalues of $\mathcal{S}_{kk}$–to be good approximations of the corresponding $\boldsymbol{s}_m^{(k)}$ since the corresponding fields do not radiate and decay rapidly outside the brick under consideration. Hence, we dub these uncoupled eigencurrents; conversely, we may also expect the lower order eigenfunctions $\boldsymbol{e}_m^{(k)}$ to depart considerably from the corresponding $\boldsymbol{s}_m^{(k)}$, so we dub them coupled eigencurrents, and we adopt $\boldsymbol{e}_m^{(k)}$ to form the set $\mathbb{E}$, naming them eigencurrents.

3.2. The algorithm

In general, we do not know the closed form of the eigenfunctions in the set $\mathbb{E}$. Thus, we achieve the solution of Eq. (5) numerically. To start, the currents $q_k^{\mathrm{s,i(F,T)}}$ on $\partial\mathcal{D}_k^{\pm\mathrm{(F,T)}}$ are expanded using a set $\mathbb{B}_k$ of $2N_f$ basis functions. The subsequent application of the MoM in Galerkin's form shall then yield the *algebraic* counterpart of Eq. (5):

$$\begin{bmatrix} \left[\boldsymbol{S}^{(\mathrm{F})}\right]^{-1} & -\left[\boldsymbol{T}^{(\mathrm{FT})}\right] \\ -\left[\boldsymbol{T}^{(\mathrm{TF})}\right] & \left[\boldsymbol{S}^{(\mathrm{T})}\right]^{-1} \end{bmatrix} \begin{bmatrix} \left[\boldsymbol{q}^{\mathrm{s(F)}}\right] \\ \left[\boldsymbol{q}^{\mathrm{s(T)}}\right] \end{bmatrix} = \begin{bmatrix} \left[\boldsymbol{q}^{\mathrm{i(F)}}\right] \\ \left[\boldsymbol{q}^{\mathrm{i(T)}}\right] \end{bmatrix}. \tag{9}$$

However, the system in Eq. (9) is not explicitly built, since it does not represent an advantage from solving the same problem using a BIE directly posed on the scatterer surfaces. Instead, we carry out the spectral

decomposition of $\left[S_{kk}^{(\mathrm{F,T})}\right]$:

$$\left[S_{kk}^{(\mathrm{F,T})}\right] = \left[V_{kk}^{(\mathrm{F,T})}\right]\left[\Lambda_{kk}^{(\mathrm{F,T})}\right]\left[V_{kk}^{(\mathrm{F,T})}\right]^{-1}, \tag{10}$$

where the diagonal matrix $\left[\Lambda_{kk}^{(\mathrm{F,T})}\right]$ contains the eigenvalues $\lambda_{lk}^{(\mathrm{F,T})}$, $l = 1, 2, \ldots, 2N_f$, arranged with their magnitudes in descending order. The sorting is also reflected in the columns of $\left[V_{kk}^{(\mathrm{F,T})}\right]$. The spectral decomposition may appear time consuming at first sight, but actually that is not necessarily the case, since it has to be done only once for bricks enclosing identical objects. Next, we proceed to form the set $\mathbb{U}^{(\mathrm{F})} \bigcup \mathbb{U}^{(\mathrm{T})}$ using $\{\boldsymbol{v}_{lk}^{(\mathrm{F,T})}\}$, i.e. the columns in $\left[V_{kk}^{(\mathrm{F,T})}\right]$, to span the spaces for $\left[\boldsymbol{q}^{\mathrm{i(F,T)}}\right]$ and $\left[\boldsymbol{q}^{\mathrm{s(F,T)}}\right]$. Hence, the set $\mathbb{U}^{(\mathrm{F})} \bigcup \mathbb{U}^{(\mathrm{T})}$ is the algebraic counterpart of $\mathbb{E}$. To reflect the spanning, we rephrase the system in Eq. (9) in this new basis, namely

$$\begin{bmatrix} \left[\check{\boldsymbol{S}}^{(\mathrm{F})}\right]^{-1} & -\left[\check{\boldsymbol{T}}^{(\mathrm{FT})}\right] \\ -\left[\check{\boldsymbol{T}}^{(\mathrm{TF})}\right] & \left[\check{\boldsymbol{S}}^{(\mathrm{T})}\right]^{-1} \end{bmatrix} \begin{bmatrix} \left[\check{\boldsymbol{q}}^{\mathrm{s(F)}}\right] \\ \left[\check{\boldsymbol{q}}^{\mathrm{s(T)}}\right] \end{bmatrix} = \begin{bmatrix} \left[\check{\boldsymbol{q}}^{\mathrm{i(F)}}\right] \\ \left[\check{\boldsymbol{q}}^{\mathrm{i(T)}}\right] \end{bmatrix}, \tag{11}$$

where

$$\begin{aligned} \left[\check{\boldsymbol{S}}^{(\mathrm{F})}\right]_{kq}^{-1} &= \left(\left[G^{(\mathrm{F})}\right]^{-1}\left[\boldsymbol{S}^{(\mathrm{F})}\right]^{-1}\left[G^{(\mathrm{F})}\right]\right)_{kq} \\ &= \begin{cases} \left[\Lambda_{kk}^{(\mathrm{F})}\right]^{-1} & k = q \\ -\left[\check{T}_{kq}^{(\mathrm{FF})}\right] & k \neq q \end{cases}, \end{aligned} \tag{12}$$

$$\begin{aligned} \left[\check{\boldsymbol{S}}^{(\mathrm{T})}\right]_{kq}^{-1} &= \left(\left[G^{(\mathrm{T})}\right]^{-1}\left[\boldsymbol{S}^{(\mathrm{T})}\right]^{-1}\left[G^{(\mathrm{T})}\right]\right)_{kq} \\ &= \begin{cases} \left[\check{S}_{kk}^{(\mathrm{T})}\right]^{-1} & k = q \\ -\left[\check{T}_{kq}^{(\mathrm{TT})}\right] & k \neq q \end{cases}, \end{aligned} \tag{13}$$

$$\left[\check{\boldsymbol{T}}^{(\mathrm{FT})}\right] = \left[G^{(\mathrm{F})}\right]^{-1}\left[\boldsymbol{T}^{(\mathrm{FT})}\right]\left[G^{(\mathrm{T})}\right], \tag{14}$$

$$\left[\check{\boldsymbol{T}}^{(\mathrm{TF})}\right] = \left[G^{(\mathrm{T})}\right]^{-1}\left[\boldsymbol{T}^{(\mathrm{TF})}\right]\left[G^{(\mathrm{F})}\right], \tag{15}$$

$$\left[\check{\boldsymbol{q}}^{\mathrm{s,i(F)}}\right] = \left[G^{(\mathrm{F})}\right]^{-1}\left[\boldsymbol{q}^{\mathrm{s,i(F)}}\right], \tag{16}$$

$$\left[\check{\boldsymbol{q}}^{\mathrm{s,i(T)}}\right] = \left[G^{(\mathrm{T})}\right]^{-1}\left[\boldsymbol{q}^{\mathrm{s,i(T)}}\right], \tag{17}$$

with $\left[G^{(\mathrm{F})}\right] = \mathrm{diag}\{\left[V_{kk}^{(\mathrm{F})}\right]\}$ and $\left[G^{(\mathrm{T})}\right] = \mathrm{diag}\{\left[V_{kk}^{(\mathrm{T})}\right]\}$ as Gram matrices [29] for the corresponding vector basis. The system of Eq. (11) together with Eqs. (12) through (17) represent the system of Eq. (9) when the eigencurrents in $\mathbb{U}^{(\mathrm{F})} \bigcup \mathbb{U}^{(\mathrm{T})}$ are used as basis and test functions. We note that even when the shape and electromagnetic properties of the target are allowed to vary, the eigencurrent basis in $\mathbb{U}^{(\mathrm{F})} \bigcup \mathbb{U}^{(\mathrm{T})}$ is held fixed;

thereby the entries in the main diagonal of $\left[\check{\boldsymbol{S}}^{(\mathrm{T})}\right]^{-1}$ in Eq. (13) are in general $\left[\check{S}_{kk}^{(\mathrm{T})}\right]^{-1}$ and not $\left[\Lambda_{kk}^{(\mathrm{T})}\right]^{-1}$ as in Eq. (12) for $\left[\check{\boldsymbol{S}}^{(\mathrm{F})}\right]^{-1}$. The main advantage of Eq. (11) over Eq. (9) is that its entries are not equally meaningful. Thus, we may further reduce the order of the system matrix without compromising the accuracy of the results, as we will show in the next section.

3.3. The order reduction technique

The system in Eq. (11) is much better than Eq. (9) for inversion because we can significantly reduce its size. To this end, we may define a permutation matrix $[P]$ ($[P]^{-1}=[P]^{\mathrm{T}}$) [29], which through a unitary transformation swaps rows and columns in Eq. (11) as described in [25]. Additionally, based on the coupled-uncoupled concept and the Gershgoring theorem [30], we may further simplify the resulting system matrix. Symbolically, this reads as

$$[P]\begin{bmatrix}\left[\check{\boldsymbol{S}}^{(\mathrm{F})}\right]^{-1} & -\left[\check{\boldsymbol{T}}^{(\mathrm{FT})}\right]\\ -\left[\check{\boldsymbol{T}}^{(\mathrm{TF})}\right] & \left[\check{\boldsymbol{S}}^{(\mathrm{T})}\right]^{-1}\end{bmatrix}[P]^{\mathrm{T}}=\begin{bmatrix}\left[\check{\boldsymbol{S}}_{\mathrm{cc}}\right]^{-1} & \left[\check{\boldsymbol{S}}_{\mathrm{cu}}\right]^{-1}\\ \left[\check{\boldsymbol{S}}_{\mathrm{uc}}\right]^{-1} & \left[\check{\boldsymbol{S}}_{\mathrm{uu}}\right]^{-1}\end{bmatrix}\approx\begin{bmatrix}\left[\check{\boldsymbol{S}}_{\mathrm{cc}}\right]^{-1} & [0]\\ [0] & \left[\check{\boldsymbol{S}}_{\mathrm{uu}}\right]^{-1}\end{bmatrix}, \tag{18}$$

with

$$\left[\check{\boldsymbol{S}}_{\mathrm{cc}}\right]^{-1}=\begin{bmatrix}\left[\check{\boldsymbol{S}}_{\mathrm{cc}}^{(\mathrm{F})}\right]^{-1} & -\left[\check{\boldsymbol{T}}_{\mathrm{cc}}^{(\mathrm{FT})}\right]\\ -\left[\check{\boldsymbol{T}}_{\mathrm{cc}}^{(\mathrm{TF})}\right] & \left[\check{\boldsymbol{S}}_{\mathrm{cc}}^{(\mathrm{T})}\right]^{-1}\end{bmatrix},\qquad \left[\check{\boldsymbol{S}}_{\mathrm{uu}}\right]^{-1}=\begin{bmatrix}\left[\boldsymbol{\Lambda}_{\mathrm{uu}}^{(\mathrm{F})}\right]^{-1} & [0]\\ [0] & \left[\check{\boldsymbol{S}}_{\mathrm{uu}}^{(\mathrm{T})}\right]^{-1}\end{bmatrix}, \tag{19}$$

where $\left[\check{\boldsymbol{S}}_{\mathrm{cc}}\right]^{-1}$ is the coupled counterpart of the matrix system in Eq. (11). This matrix explicitly states that the coupled eigencurrents play the predominant role in accounting for the multiple scattering taking place among the bricks inside the fixed structure and the target, and between them. Furthermore, $\left[\boldsymbol{\Lambda}_{\mathrm{uu}}^{(\mathrm{F})}\right]^{-1}$ is a diagonal matrix that contains all the eigenvalues corresponding to all uncoupled eigencurrents in $\mathbb{U}^{(\mathrm{F})}$, and $\left[\check{\boldsymbol{S}}_{\mathrm{uu}}^{(\mathrm{T})}\right]^{-1}$ is a block diagonal matrix that contains the uncoupled entries of each $\left[\check{S}_{kk}^{(\mathrm{T})}\right]^{-1}$. At this point, we have transformed our problem into the following:

- The formal solution of a system whose matrix given by the leftmost in Eq. (19) has a size far smaller, since only $N_{\mathrm{c}}(N_{\mathrm{T}}+N_{\mathrm{B}})$ with $N_{\mathrm{c}}\ll 2N_f$ eigencurrents instead of the original $2N_f(N_{\mathrm{B}}+N_{\mathrm{T}})$ are likely to be coupled.
- The direct solution of a system whose matrix given by the rightmost in Eq. (19) is block diagonal.

Only at the end –when both systems have been solved– do we revert to the original basis by taking into account all the eigencurrents. Thereby, the expansion coefficients of $\left[\boldsymbol{q}^{\mathrm{s(F,T)}}\right]$ in the original basis $\bigcup\mathbb{B}_k$ may be written with the help of Eq. (19) as

$$\begin{bmatrix}\left[\boldsymbol{q}^{\mathrm{s(F)}}\right]\\ \left[\boldsymbol{q}^{\mathrm{s(T)}}\right]\end{bmatrix}\approx[G]\,[P]^{\mathrm{T}}\begin{bmatrix}\left[\check{\boldsymbol{S}}_{\mathrm{cc}}\right] & [0]\\ [0] & \left[\check{\boldsymbol{S}}_{\mathrm{uu}}\right]\end{bmatrix}[P]\,[G]^{-1}\begin{bmatrix}\left[\boldsymbol{q}^{\mathrm{i(F)}}\right]\\ \left[\boldsymbol{q}^{\mathrm{i(T)}}\right]\end{bmatrix}, \tag{20}$$

which is the sought solution of Eq. (9). Furthermore, by also applying the described procedure to both right-hand sides in Eqs. (3) and (4), we obtain the total equivalent incident currents $\left[\boldsymbol{q}_{\mathrm{tot}}^{\mathrm{i(F,T)}}\right]$ as

$$\begin{bmatrix}\begin{bmatrix}\boldsymbol{q}_{\mathrm{tot}}^{\mathrm{i(F)}}\\ \boldsymbol{q}_{\mathrm{tot}}^{\mathrm{i(T)}}\end{bmatrix}\end{bmatrix}\approx[G]\,[P]^{\mathrm{T}}\begin{bmatrix}[\boldsymbol{\Lambda}_{\mathrm{cc}}]^{-1}[\check{\boldsymbol{S}}_{\mathrm{cc}}] & [0]\\ [\check{\boldsymbol{T}}_{\mathrm{uc}}]\,[\check{\boldsymbol{S}}_{\mathrm{cc}}] & [\mathrm{I}]\end{bmatrix}[P]\,[G]^{-1}\begin{bmatrix}[\boldsymbol{q}^{\mathrm{i(F)}}]\\ [\boldsymbol{q}^{\mathrm{i(T)}}]\end{bmatrix}, \tag{21}$$

where [I] is the identity matrix, $[\boldsymbol{\Lambda}_{\mathrm{cc}}]^{-1}$ is the coupled counterpart of $[\check{\boldsymbol{S}}_{\mathrm{uu}}]^{-1}$, i.e. $\mathrm{diag}\{\left[\boldsymbol{\Lambda}_{\mathrm{cc}}^{(\mathrm{F})}\right]^{-1},\left[\check{\boldsymbol{S}}_{\mathrm{cc}}^{(\mathrm{T})}\right]^{-1}\}$, $[G]=\mathrm{diag}\{\left[G^{(\mathrm{F})}\right],\left[G^{(\mathrm{T})}\right]\}$, and $\left[\check{\boldsymbol{T}}_{\mathrm{uc}}\right]$ is a transfer matrix from the coupled to the uncoupled eigencurrents in the set $\mathbb{U}^{(\mathrm{F})}\bigcup\mathbb{U}^{(\mathrm{T})}$. Further manipulation of the matrices in Eq. (19) provides the sought set of equations for optimization purposes:

$$\left[\left[\check{\boldsymbol{S}}_{\mathrm{cc}}^{(\mathrm{T})}\right]^{-1}-\left[\check{\boldsymbol{S}}_{\mathrm{cc}}^{(\mathrm{T/F})}\right]\right]\left[\check{\boldsymbol{q}}_{\mathrm{c}}^{\mathrm{s(T)}}\right]=\left[\check{\boldsymbol{q}}_{\mathrm{c}}^{\mathrm{i(T)}}\right]+\left[\check{\boldsymbol{q}}_{\mathrm{c}}^{\mathrm{i(T/F)}}\right], \tag{22}$$

$$\left[\check{\boldsymbol{S}}_{\mathrm{uu}}^{(\mathrm{T})}\right]^{-1}\left[\check{\boldsymbol{q}}_{\mathrm{u}}^{\mathrm{s(T)}}\right]=\left[\check{\boldsymbol{q}}_{\mathrm{u}}^{\mathrm{i(T)}}\right], \tag{23}$$

with

$$\left[\check{\boldsymbol{S}}_{\mathrm{cc}}^{(\mathrm{T/F})}\right]=\left[\check{\boldsymbol{T}}_{\mathrm{cc}}^{(\mathrm{TF})}\right]\left[\check{\boldsymbol{S}}_{\mathrm{cc}}^{(\mathrm{F})}\right]\left[\check{\boldsymbol{T}}_{\mathrm{cc}}^{(\mathrm{FT})}\right], \tag{24}$$

$$\left[\check{\boldsymbol{q}}_{\mathrm{c}}^{\mathrm{i(T/F)}}\right]=\left[\check{\boldsymbol{T}}_{\mathrm{cc}}^{(\mathrm{TF})}\right]\left[\check{\boldsymbol{S}}_{\mathrm{cc}}^{(\mathrm{F})}\right]\left[\check{\boldsymbol{q}}_{\mathrm{c}}^{\mathrm{i(F)}}\right], \tag{25}$$

where $\left[\check{\boldsymbol{S}}_{\mathrm{cc}}^{(\mathrm{T/F})}\right]$ is the scattering operator of the fixed part as seen from the target in the coupled basis and $\left[\check{\boldsymbol{q}}_{\mathrm{c}}^{\mathrm{i(T/F)}}\right]$ is the additional incident current impinging on the target due to the presence of the fixed part. The system of Eqs. (22) and (23) is a size-reduced system that efficiently encompasses electromagnetically the presence of the fixed part in the vicinity of the target and they explicitly state that in order to optimize a compact designated domain (i.e. the target structure) inside a large fixed structure, we must only recompute $\left[\check{S}_{kk}^{(\mathrm{T})}\right]$ when a parameter changes in the target, and this is a welcome effect of the diakoptic nature of LEGO.

We additionally observe that the matrices $\left[\check{\boldsymbol{S}}_{\mathrm{cc}}^{(\mathrm{T/F})}\right]$ and $\left[\check{\boldsymbol{q}}_{\mathrm{c}}^{\mathrm{i(T/F)}}\right]$ in Eq. (22) as stated in Eqs. (24) and (25) require the formal inversion of $\left[\check{\boldsymbol{S}}_{\mathrm{cc}}^{(\mathrm{F})}\right]^{-1}$, which can be numerically unstable. This observation is corroborated by the fact that the amplitude range of the entries in $\left[\check{\boldsymbol{S}}_{\mathrm{cc}}^{(\mathrm{F})}\right]^{-1}$ coming from any 2 coupled eigencurrents in $\mathbb{U}^{(\mathrm{F})}$ may span several orders of magnitude as the amplitudes of the corresponding eigenvalues. Therefore, a scaling procedure is decisive to compute $\left[\check{\boldsymbol{S}}_{\mathrm{cc}}^{(\mathrm{F})}\right]$ accurately and consequently obtain the solution of Eq. (22).

3.4. Well-balanced matrix system for optimization

We start by observing that $\left[\check{\boldsymbol{S}}_{\mathrm{cc}}^{(\mathrm{F})}\right]^{-1} = \left[\boldsymbol{\Lambda}_{\mathrm{cc}}^{(\mathrm{F})}\right]^{-1} - \left[\check{\boldsymbol{T}}_{\mathrm{cc}}^{(\mathrm{FF})}\right]$ where $\left[\boldsymbol{\Lambda}_{\mathrm{cc}}^{(\mathrm{F})}\right]^{-1}$ is a diagonal matrix that contains the inverse of all coupled eigenvalues in $\mathbb{U}^{(\mathrm{F})}$ and $\left[\check{\boldsymbol{T}}_{\mathrm{cc}}^{(\mathrm{FF})}\right]$ contains the transfer matrices among the bricks in the fixed structure in the coupled eigencurrent basis of $\mathbb{U}^{(\mathrm{F})}$. By extracting $\left[\boldsymbol{\Lambda}_{\mathrm{cc}}^{(\mathrm{F})}\right]^{-1}$ as a factor, we may write

$$\left[\check{\boldsymbol{S}}_{\mathrm{cc}}^{(\mathrm{F})}\right] = \left([\mathrm{I}] - \left[\boldsymbol{\Lambda}_{\mathrm{cc}}^{(\mathrm{F})}\right]\left[\check{\boldsymbol{T}}_{\mathrm{cc}}^{(\mathrm{FF})}\right]\right)^{-1}\left[\boldsymbol{\Lambda}_{\mathrm{cc}}^{(\mathrm{F})}\right]. \tag{26}$$

The matrix $\left[\boldsymbol{E}_{\mathrm{cc}}^{(\mathrm{F})}\right] \equiv \left([\mathrm{I}] - \left[\boldsymbol{\Lambda}_{\mathrm{cc}}^{(\mathrm{F})}\right]\left[\check{\boldsymbol{T}}_{\mathrm{cc}}^{(\mathrm{FF})}\right]\right)$ is more suitable for "inversion" since $\left[\boldsymbol{\Lambda}_{\mathrm{cc}}^{(\mathrm{F})}\right]$ acts as a row-scaling diagonal matrix over the entries of $\left[\check{\boldsymbol{T}}_{\mathrm{cc}}^{(\mathrm{FF})}\right]$; moreover, $\left[\boldsymbol{\Lambda}_{\mathrm{cc}}^{(\mathrm{F})}\right]$ at the rightmost of (26) will do the same scaling to any other matrix when it is left multiplied by Eq. (26). Upon multiplication of Eq. (22) by $\mathrm{diag}\{\left[\check{S}_{kk,\mathrm{cc}}^{(\mathrm{T})}\right]\}$ (i.e. a block diagonal matrix formed with the coupled entries of each $\left[\check{S}_{kk}^{(\mathrm{T})}\right]$), we get the sought well-balanced system matrix:

$$\left[\left[\hat{\boldsymbol{S}}_{\mathrm{cc}}^{(\mathrm{T})}\right]^{-1} - \left[\hat{\boldsymbol{S}}_{\mathrm{cc}}^{(\mathrm{T/F})}\right]\right]\left[\check{\boldsymbol{q}}_{\mathrm{c}}^{\mathrm{s}(\mathrm{T})}\right] = \left[\hat{\boldsymbol{q}}_{\mathrm{c}}^{\mathrm{i}(\mathrm{T})}\right] + \left[\hat{\boldsymbol{q}}_{\mathrm{c}}^{\mathrm{i}(\mathrm{T/F})}\right], \tag{27}$$

with

$$\left[\hat{\boldsymbol{S}}_{\mathrm{cc}}^{(\mathrm{T})}\right]^{-1} = \left([\mathrm{I}] - \mathrm{diag}\{\left[\check{S}_{kk,\mathrm{cc}}^{(\mathrm{T})}\right]\}\left[\check{\boldsymbol{T}}_{\mathrm{cc}}^{(\mathrm{TT})}\right]\right), \tag{28}$$

$$\left[\hat{\boldsymbol{S}}_{\mathrm{cc}}^{(\mathrm{T/F})}\right] = \left[\hat{\boldsymbol{T}}_{\mathrm{cc}}^{(\mathrm{TF})}\right]\left[\boldsymbol{E}_{\mathrm{cc}}^{(\mathrm{F})}\right]^{-1}\left[\hat{\boldsymbol{T}}_{\mathrm{cc}}^{(\mathrm{FT})}\right], \tag{29}$$

$$\left[\hat{\boldsymbol{q}}_{\mathrm{c}}^{\mathrm{i}(\mathrm{T})}\right] = \mathrm{diag}\{\left[\check{S}_{kk,\mathrm{cc}}^{(\mathrm{T})}\right]\}\left[\check{\boldsymbol{q}}_{\mathrm{c}}^{\mathrm{i}(\mathrm{T})}\right], \tag{30}$$

$$\left[\hat{\boldsymbol{q}}_{\mathrm{c}}^{\mathrm{i}(\mathrm{T/F})}\right] = \left[\hat{\boldsymbol{T}}_{\mathrm{cc}}^{(\mathrm{TF})}\right]\left[\boldsymbol{E}_{\mathrm{cc}}^{(\mathrm{F})}\right]^{-1}\left[\boldsymbol{\Lambda}_{\mathrm{cc}}^{(\mathrm{F})}\right]\left[\check{\boldsymbol{q}}_{\mathrm{c}}^{\mathrm{i}(\mathrm{F})}\right], \tag{31}$$

$$\left[\hat{\boldsymbol{T}}_{\mathrm{cc}}^{(\mathrm{TF})}\right] = \mathrm{diag}\{\left[\check{S}_{kk,\mathrm{cc}}^{(\mathrm{T})}\right]\}\left[\check{\boldsymbol{T}}_{\mathrm{cc}}^{(\mathrm{TF})}\right], \tag{32}$$

$$\left[\hat{\boldsymbol{T}}_{\mathrm{cc}}^{(\mathrm{FT})}\right] = \left[\boldsymbol{\Lambda}_{\mathrm{cc}}^{(\mathrm{F})}\right]\left[\check{\boldsymbol{T}}_{\mathrm{cc}}^{(\mathrm{FT})}\right]. \tag{33}$$

3.5. Numerical features of LEGO and the EEM

The LEGO approach endowed with the EEM expansion method has remarkable numerical features that are worthwhile to mention. Specifically, we observe in Eqs. (19), (20), (21), (23), and (27) that:

1. When building $\left[\check{\boldsymbol{S}}_{\mathrm{cc}}^{(\mathrm{F})}\right]^{-1}$ and $\left[\check{\boldsymbol{S}}_{\mathrm{cc}}^{(\mathrm{T})}\right]^{-1}$, the matrices $\left[\check{T}_{kq}^{(\mathrm{FF})}\right]$, $\left[\check{T}_{kq}^{(\mathrm{TT})}\right]$, $\left[\check{T}_{qk}^{(\mathrm{FF})}\right]$, and $\left[\check{T}_{qk}^{(\mathrm{TT})}\right]$ are computed, but we only retain the entries corresponding to coupled eigencurrents, whereas the rest is disregarded. The same applies to the global transfer matrices $\left[\check{\boldsymbol{T}}_{\mathrm{cc}}^{(\mathrm{FT})}\right]$ and $\left[\check{\boldsymbol{T}}_{\mathrm{cc}}^{(\mathrm{TF})}\right]$.

2. Since the eigencurrent basis $\mathbb{U}^{(\mathrm{F})} \bigcup \mathbb{U}^{(\mathrm{T})}$ is fixed, we may exploit the translational symmetry among the bricks in the computation of the transfer matrices in order to reduce the computational cost since most of the transfer matrices would coincide.

3. $\left[\check{\boldsymbol{S}}_{\mathrm{uu}}\right]^{-1}$ in Eq. (19) is neither built nor inverted, since we compute the eigenvalues $\lambda_{lk}^{(\mathrm{F})}$ of $\left[\Lambda_{kk}^{(\mathrm{F})}\right]$ and $\left[\check{S}_{kk}^{(\mathrm{T})}\right]$ directly.

4. The permutation matrix $[P]$ and the Gram matrix $[G]$ are never built. In fact, to compute $\left[\check{\boldsymbol{q}}_{\mathrm{c,u}}^{\mathrm{i,s}}\right]$ either on the fixed structure or the target we do solve $N_{\mathrm{B}}+N_{\mathrm{T}}$ systems of the form $[V_{kk}]\left[\check{q}_k^{\mathrm{i,s}}\right]=\left[q_k^{\mathrm{i,s}}\right]$ and detach each $\left[\check{q}_k^{\mathrm{i,s}}\right]$ in its coupled and uncoupled parts.

5. Finally, with regard to the optimization, the matrices $\left[\hat{\boldsymbol{S}}_{\mathrm{cc}}^{(\mathrm{T/F})}\right]$, $\left[\hat{\boldsymbol{q}}_{\mathrm{c}}^{\mathrm{i(T/F)}}\right]$, $\left[\hat{\boldsymbol{q}}_{\mathrm{c}}^{\mathrm{i(T)}}\right]$, and $\left[\check{\boldsymbol{q}}_{\mathrm{u}}^{\mathrm{i(T)}}\right]$ are computed only once for all possible varying parameters of the target. Just $\left[\check{S}_{kk}^{(\mathrm{T})}\right]$ has to be recomputed to update $\left[\hat{\boldsymbol{S}}_{\mathrm{cc}}^{(\mathrm{T})}\right]$ and $\left[\check{\boldsymbol{S}}_{\mathrm{uu}}^{(\mathrm{T})}\right]$.

4. Optimization of a 2-D EBG polarization splitter

Let us consider a numerical example with potentially interesting applications. In particular, let us employ the LEGO-EEM to tune a 2-D EBG polarization splitter as described in Section 3. To design the EBG polarization splitter, the basic EBG structure must exhibit a full band-gap over the operating frequency, i.e. there must be an overlapping band-gap for both polarizations, namely TM_z and TE_z. We employ a triangular arrangement of air holes with filling ratio $r/a=0.45$ in a dielectric material with relative permittivity $\varepsilon_r=11.56$. This structure presents a full band-gap for normalized frequencies in the range of $0.41\leq f\frac{a}{c}\leq 0.45$ [31]. To separate the polarizations, 3 defect waveguides with polarization-dependent modes are introduced in the basic photonic crystal, forming a Y branch as shown in Figure 2. The defect waveguides are designed in such a way that the output waveguides support only one polarization each, while the input waveguide supports both. The propagating mode that the defect waveguides can support depends on the chosen defect radius. In particular, for a defect radius $r/a=0.33$, the input waveguide supports modes of both polarizations in the band-gap, whereas one output waveguide with a defect radius of $r/a=0.24$ supports only TE_z modes in a frequency range of $0.430\leq f\frac{c}{a}\leq 0.434$, and the other output waveguide with defect radius $r/a=0.19$ supports only TM_z modes in the same frequency range.

For the EBG polarization splitter in Figure 2, we aim at tuning the target structure both in permittivity ε_i and filling factor r_i/a to minimize the polarization coupling between the TM_z and TE_z waveguides. The polarization coupling is defined as

$$C^{\mathrm{TM}_z}=\frac{P^{\mathrm{TE}_z|\mathrm{TM}_z}}{P^{\mathrm{TM}_z|\mathrm{TM}_z}},\qquad C^{\mathrm{TE}_z}=\frac{P^{\mathrm{TM}_z|\mathrm{TE}_z}}{P^{\mathrm{TE}_z|\mathrm{TE}_z}},\tag{34}$$

where $\frac{P^{\mathrm{TE}_z|\mathrm{TM}_z}}{P^{\mathrm{TM}_z|\mathrm{TM}_z}}$ ($\frac{P^{\mathrm{TM}_z|\mathrm{TE}_z}}{P^{\mathrm{TE}_z|\mathrm{TE}_z}}$) is the ratio between the power that flows through the TE_z (TM_z) waveguide and the power that flows through the TM_z (TE_z) waveguide when a TM_z (TE_z) polarized mode is excited in the input waveguide. These powers are monitored using 2 sensor cells as depicted in Figure 2. The sensor cells can be easily incorporated into the target without additional computational cost as long as their content, i.e. the material and cylinders inside them, are kept constant throughout the optimization. We define our cost function using both polarization couplings, and we tune the target structure in Figure 2 by searching for

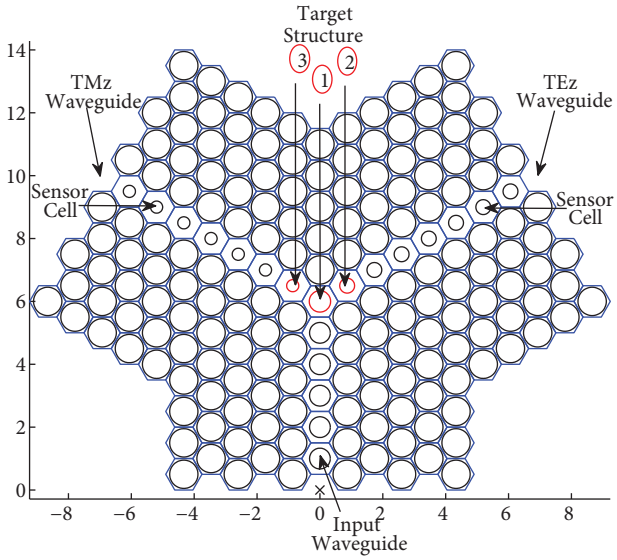

Figure 2. 2-D EBG polarization splitter consisting of 3 defect waveguides with polarization-dependent modes. Each cylinder has been embedded in as many hexagonal bricks. The target to be optimized is highlighted with red cylinders.

$\boldsymbol{u}^\star = \left(r_1^\star/a, \ldots, r_{N_\mathrm{T}}^\star/a, \varepsilon_1^\star, \ldots, \varepsilon_{N_\mathrm{T}}^\star\right) \in \mathbb{R}^+$ such that

$$\mathrm{CF}(\boldsymbol{u}^\star) = \min_{\boldsymbol{u}}\{C^{\mathrm{TM}z} + C^{\mathrm{TE}z}\}. \tag{35}$$

4.1. Numerical results

To proceed with the optimization, we set $a = 1\,\mathrm{mm}$, $f = 0.432\frac{c}{a} = 129.6\,\mathrm{GHz}$, and an initial estimate of $\boldsymbol{u}_o = (0.5, 0.5, 0.5, 5, 5, 5)$. We confine the searching space such that $\varepsilon_0 \leq \varepsilon_i \leq 40\varepsilon_0$ and $0 \leq \frac{r_i}{a} \leq 0.5$. The whole fixed structure is composed of $N_\mathrm{B} = 186$ hexagonal bricks and is discretized using $2N_f N_\mathrm{B} = 24552$ triangle basis functions. In a similar fashion, for the target structure we have $N_\mathrm{T} = 3$ for $2N_f N_\mathrm{T} = 396$ triangle basis functions. We use $N_\mathrm{o} = 100$ triangle basis functions over each cylinder contour to compute $\left[S_{kk}^{(\mathrm{F,T})}\right]$. To compute $\left[\check{\boldsymbol{S}}_{\mathrm{cc}}^{(\mathrm{T/F})}\right]$ and $\left[\check{\boldsymbol{q}}_{\mathrm{c}}^{\mathrm{i}(\mathrm{T/F})}\right]$ —see Eqs. (24) and (25)— we retain $N_\mathrm{c} = 100$ coupled eigencurrents per brick for both the fixed and the target structure. Accordingly, the sizes of these matrices shrink down to $N_\mathrm{c}N_\mathrm{T} \times N_\mathrm{c}N_\mathrm{T} = 300 \times 300$ as compared to $2N_f N_\mathrm{T} \times 2N_f N_\mathrm{T} = 396 \times 396$ for a gained compression of 43%. The reason why the retained number of coupled eigencurrents per brick $N_\mathrm{c} = 100$ is comparable to the number of basis functions per brick $2N_f = 132$ is that most of the circular cylinders in the polarization splitter have a high filling factor, i.e. they are almost filling completely the hexagonal bricks. As a consequence, the spectrum of $\left[S_{kk}^{(\mathrm{F})}\right]$ for these cylinders broadens, thereby considerably increasing the lower bound for the number of coupled eigencurrents that are to be retained. Finally, we choose to optimize our cost function in Eq. (35) using a quasi-Newton algorithm, as implemented in the subroutine `E04JYF` of the `Mark 21 NAG` library. To this end, we compute each polarization coupling exciting the structure with 2 different sources. Hence, we use a unitary electric line source along z at input to excite a TM_z mode, whereas the TE_z mode is excited using a unitary notional magnetic line source along z.

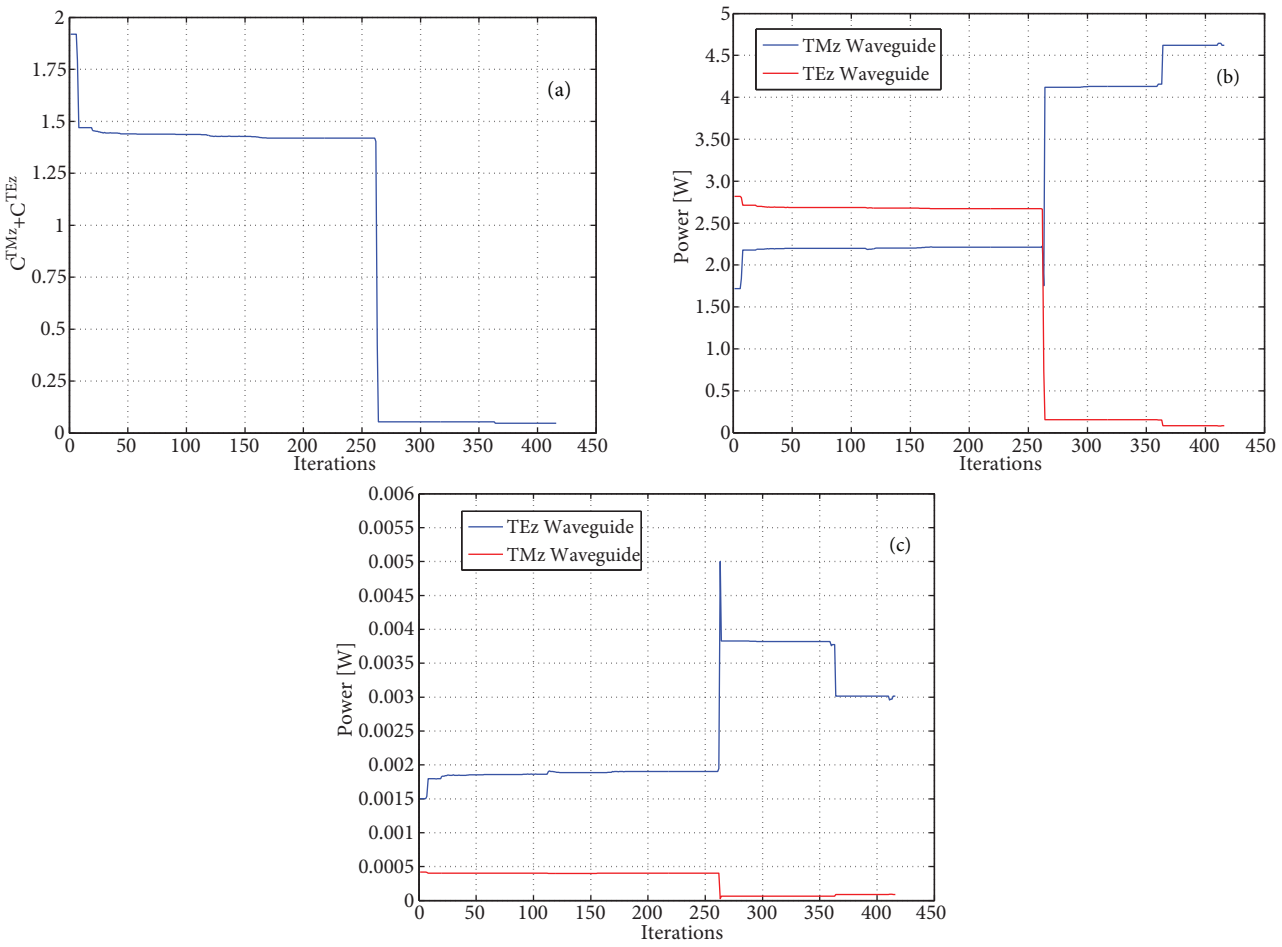

Figure 3. (a) The cost function CF vs. the number of iterations. (b) and (c) The sensed power in the waveguides vs. the number of iterations when a TM_z-TE_z polarized mode is excited in the input waveguide.

Figure 3(a) shows the CF versus the number of iterations during the optimization. Convergence was reached after $N_\mathrm{i} = 416$ iterations, for a cost function $\mathrm{CF}(\boldsymbol{u}^\star) = 0.047$ with $\boldsymbol{u}^\star = (0.296, 0.200, 0.297, 9.36\varepsilon_0, 1.1\varepsilon_0, 9.65\varepsilon_0)$. Figures 3(b) and 3(c) show the power flowing through the output waveguides for TM_z and TE_z excitations in the input waveguide, respectively. Note that different scales in the vertical axis are used for the sensed output power in both plots, for different sources are exciting the structure at each polarization, as we previously mentioned. We observe therein that a minimization of the overall cost function does not imply evidently an individual minimization of C^{TM_z} and C^{TE_z}. At $\boldsymbol{u} = \boldsymbol{u}^\star$, we have $C^{\mathrm{TM}_z}\big|_{\boldsymbol{u}=\boldsymbol{u}^\star} \approx \frac{1}{56}$ and $C^{\mathrm{TE}_z}\big|_{\boldsymbol{u}=\boldsymbol{u}^\star} \approx \frac{1}{34}$.

Figure 4 shows a snapshot of the field distribution in the 2-D EBG polarization splitter after optimization. The fields have been computed through the total equivalent incident currents given by Eq. (21) and the relevant dyadic Green's functions of the bricks, exciting the splitter with the very sources during the optimization. Thus, the Figure 4(a) shows the longitudinal electric field $|\boldsymbol{E_z}|$, while Figure 4(b) shows the longitudinal magnetic field $|\boldsymbol{H_z}|$. Again, different scales are necessary in both snapshots. The continuity of the fields across the hexagonal contours, where the equivalent incident currents are defined, is a good test for the validity of our approach. The snapshot demonstrates the functionality of the polarization splitter. We also observe that the confinement

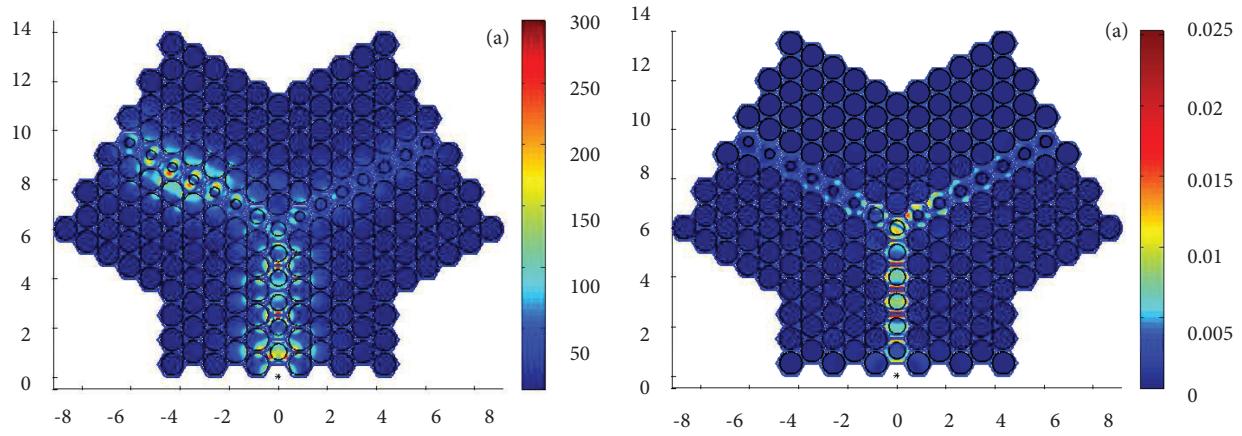

Figure 4. (a) $|\boldsymbol{E_z}|$ in the 2-D EBG polarization splitter after optimization when a TM_z polarized mode is excited in the input waveguide. (b) $|\boldsymbol{H_z}|$ in the 2-D EBG polarization splitter after optimization when a TE_z polarized mode is excited in the input waveguide.

of the TE_z guided mode is stronger than that of the TM_z guided mode. Therefore, we may expect a TE_z band-gap broader than its TM_z counterpart. One should bear in mind that there is strong mismatch at the transition from any output waveguide into the background medium. Such mismatch reduces the performance of the polarization splitter and consequently the optimization in general.

5. Conclusions

We have proposed an efficient method based on LEGO and the EEM for the numerical modeling and optimization of 2-D EBG structures. The method uses Love's equivalence principle to tear apart a composite structure into bricks. The bricks may be of arbitrary shape, which adds flexibility in the assembling of separate regions. We have formulated the optimization deriving a system of equations involving the total inverse scattering operators of the interacting structures and global transfer operators among them. We then compressed the algebraic system using the EEM, and finally a reduced matrix system involving the scattering operator of the fixed structure as seen from the target was used to effectively optimize the latter. The approach reduces the memory requirements by orders of magnitudes. A numerical test involving a 2-D EBG polarization splitter was carried out, demonstrating that LEGO-EEM can perform much better than the standard MoM for a specific class of EM problems, especially for configurations with many identical bricks/elements/cells. We have also seen that LEGO-EEM lends itself to parallelization as most of the transfer matrices among the bricks can be computed independently.

Acknowledgments

This research was supported by the MEMPHIS project under contract no., 10006758.

References

[1] F. Frezza, L. Pajewski, G. Schettini, "Characterization and design of two-dimensional electromagnetic band-gap structures by use of a full-wave method for diffraction gratings", IEEE Transactions on Microwave Theory and Techniques, Vol. 51, pp. 941–951, 2003.

[2] K.M. Ho, C.T. Chan, C.M. Soukoulis, "Existence of a photonic gap in periodic dielectric structures", Physical Review Letters, Vol. 65, pp. 3152–3155, 1990.

[3] P. Bell, J. Pendry, L. Moreno, A. Ward, "A program for calculating photonic band structures and transmission coefficients of complex structures", Computer Physics Communications, Vol. 85, pp. 306–322, 1995.

[4] A. Reynolds, H. Chong, I. Thayne, J. Arnold, P. de Maagt, "Angular frequency dependence for a planar cavity defect introduced into a 2-dimensional photonic crystal", IEEE Transactions on Microwave Theory and Techniques, Vol. 49, pp. 1254–1261, 2001.

[5] A.M. van de Water, B.P. de Hon, M.C. van Beurden, A.G. Tijhuis, P. de Maagt, "Linear embedding via Green's operators: A modeling technique for finite electromagnetic band-gap structures", Physical Review E, Vol. 72, pp. 56704–56715, 2005.

[6] K.S. Yee, "Numerical solution of initial boundary value problems involving Maxwell's equations in isotropic media", IEEE Transactions on Antennas and Propagation, Vol. 14, pp. 302–307, 1966.

[7] D. Smith, S. Schultz, N. Kroll, "Experimental and theoretical results for two-dimensional metal photonic band-gap cavity", Applied Physics Letters, Vol. 65, pp. 645–647, 1994.

[8] X. Hui Wu, A.A. Kishk, A.W. Glisson, "A transmission line method to compute the far-field radiation of arbitrarily directed Hertzian dipoles in a 1-D EBG structure", IEEE Transactions on Antennas and Propagation, Vol. 54, pp. 2731–2741, 2006.

[9] C.A. Balanis, Advanced Engineering Electromagnetics, New York, John Wiley & Sons, 1989.

[10] R.C. Hall, R. Mittra, K.M. Mitzner, "Analysis of multilayered periodic structures using generalized scattering matrix", IEEE Transactions on Antennas and Propagation, Vol. 36, pp. 111–117, 1988.

[11] M. Hammer, O.V. Ivanova, "Effective index approximations of photonic crystal slabs:a 2-to-1-D assessment", Optical and Quantum Electronics, Vol. 41, pp. 267–283, 2009.

[12] O.V. Ivanova, R. Stoffer, L. Kauppinen, M. Hammer, "Variational effective method for 3-D vectorial scattering problems in photonics: TE polarization", Progress in Electromagnetics Research Symposium, pp. 1038–1042, 2009.

[13] O.V. Ivanova, R. Stoffer, M. Hammer, "A dimensionality reduction technique for 2-D scattering problems in photonics", Journal of Optics, Vol. 12, pp. 035502–035517, 2010.

[14] P. Lalanne, "Effective medium theory applied to photonic crystals composed of cubic or square cylinders", Applied Optics, Vol. 35, pp. 5369–5380, 1996.

[15] D.H.Y. Yang, "Theory of antenna radiation from photonic band-gap materials", Electromagnetics, Vol. 19, pp. 255–276, 1999.

[16] O.C. Zienkienwicz, The Finite Element Method in Engineering Science, London, McGraw-Hill, 1971.

[17] T. Suzuki, P.K.L. Yu, "Emission power of an electric dipole in the photonic band structure of the FCC lattice", Journal of the Optical Society of America B, Vol. 12, pp. 570–582, 1995.

[18] G. Krohn, "A set of principles to interconnect the solutions of physical systems", Journal of Applied Physics, Vol. 24, pp. 965–980, 1953.

[19] S.R. Rengarajan, Y.R. Samii, "The field equivalence principle: illustration of the establishment of the non-intuitive null fields", IEEE Transactions on Antennas and Propagation, Vol. 42, pp. 122–128, 2000.

[20] S.A. Schelkunoff, "Some equivalence theorems of electromagnetics and their application to radiation problems", Bell System Technical Journal, Vol. 15, pp. 92–112, 1936.

[21] W.C. Chew, C.C. Lu, "The use of Huygens' equivalence principle for solving the volume integral equation of scattering", IEEE Transactions on Antennas and Propagation, Vol. 41, pp. 897–904, 1993.

[22] M.K. Li, W.C. Chew, "Wave-field interaction with complex structures using equivalence principle algorithm", IEEE Transactions on Antennas and Propagation, Vol. 55, pp. 130–138, 2007.

[23] D. Duque, V. Lancellotti, B.P. de Hon, A.G. Tijhuis, "Scattering from truncated cylinders with a mixed 2-D/3-D domain decomposition scheme", 6th European Conference of Antennas and Propagation, 26–30 March 2012, Prague, pp. 2660–2663, 2012.

[24] D. Duque, V. Lancellotti, B.P. de Hon, A.G. Tijhuis, "Eigencurrent expansion and linear embedding via Green's operators applied to design optimization of devices in electromagnetic band-gap structures", XXX URSI General Assembly and Scientific Symposium, 13–20 August, İstanbul, 2011.

[25] V. Lancellotti, B.P. de Hon, A.G. Tijhuis, "An eigencurrent approach to the analysis of electrically large 3-D structures using LEGO", IEEE Transactions on Antennas and Propagation, Vol. 57, pp. 3575–3585, 2009.

[26] G. Goubau, N.N. Puri, F. Schwering, "Diakoptic theory of multielement antennas", IEEE Transactions on Antennas and Propagation, Vol. 30, pp. 15–26, 1982.

[27] F. Schwering, N.N. Puri, C.M. Butler, "Modified diakoptic theory of antennas", IEEE Transactions on Antennas and Propagation, Vol. 34, pp. 1273–1281, 1986.

[28] D. Duque, V. Lancellotti, B. P. de Hon, "Combined LEGO-eigencurrent approach for enhanced solution of electrically large 2-D EBG structures", 4th European Conference of Antennas and Propagation, 12–16 April 2010, Barcelona, pp. 1–5, 2010.

[29] L.N. Trefethen, D. Bau 3rd, Numerical Linear Algebra. Philadelphia, SIAM, 1997.

[30] Y. Saad, Iterative Methods for Sparse Linear Systems. Philadelphia, SIAM, 2003.

[31] V. Rinnerbauer, J. Schermer, K. Hingerl, "Polarization splitting based on planar photonic crystals", Proceedings of ECOC 2004 We2.1.3, pp. 97–100, 2004.